Journal of Computational Mathematics and Physics
www.jcmp.org

Article Type: Original Research Article

An Uncertainty-Aware Physics-Informed Neural Network Framework for Nonlinear Fractional Partial Differential Equations in Mathematical Physics

Muhammad Umar [1,2,*]

[1]Center for Applied Mathematics and Bioinformatics, Department of Mathematics and Natural Sciences, Gulf University for Science and Technology Mubarak Al-Abdullah Area/West Mishref, Kuwait.
[2]The CA-AD Group, Heidelberg University, Germany.

*Corresponding Author: muhammad.umar@alumni.uni-heidelberg.de

Received: 24 March 2026 **Accepted:** 01 July 2026 **Published:** 09 July 2026

Abstract

This study develops a stochastic fractional extension of the two-mode Nizhnik–Novikov–Veselov (TMNNV) equation and investigates the combined influence of memory, nonlinear dispersion, deterministic forcing, and environmental noise on nonlinear wave propagation. A Caputo time-fractional operator is used to represent hereditary effects, while both additive and multiplicative Gaussian perturbations are introduced to model unresolved fluctuations in optical, plasma, and fluid media. A fractional traveling-wave reduction transforms the governing stochastic partial differential equation into a randomly forced planar system with a cubic Hamiltonian potential. The deterministic skeleton is classified through equilibrium analysis, first integrals, homoclinic and periodic orbits, and codimension-one bifurcation conditions. The stochastic dynamics are then examined by means of Itô generators, Lyapunov functions, mean-square bounds, stochastic averaging, stationary densities, finite-time Lyapunov exponents, Poincaré sections, and noise-dependent bifurcation diagrams. Analytical criteria are established for local stochastic stability, practical mean-square boundedness, and noise-induced switching between coexisting wave states. Exact deterministic bright–dark solitary and elliptic periodic waves are recovered as the zero-noise limit, thereby providing benchmark profiles for numerical validation. A reproducible computational protocol based on a predictor–corrector discretization for the fractional term and an Euler–Maruyama update for the stochastic subsystem is formulated. Representative parameter studies show how increasing noise intensity broadens the invariant density, shifts effective bifurcation thresholds, promotes intermittent transitions, and may create positive finite-time Lyapunov exponents in regimes that are regular in the deterministic model. The proposed framework extends deterministic bifurcation studies of the fractional TMNNV model and provides a unified basis for studying random wave switching, stochastic resonance, and uncertainty-aware control in nonlinear mathematical physics.

Keywords: Fractional TMNNV equation, stochastic partial differential equation, noise-induced bifurcation, chaos, soliton, Lyapunov exponent, multistability, Caputo derivative.

1. Introduction

Nonlinear evolution equations are central mathematical tools for describing coherent structures, dispersive waves, pattern formation, and instability in plasma physics, fluid mechanics, nonlinear optics, elastic media, and condensed-matter systems. Classical integrable and near-integrable models such as the Korteweg–de Vries, nonlinear Schrödinger, Kadomtsev–Petviashvili, and Nizhnik–Novikov–Veselov equations provide canonical descriptions of the balance between nonlinearity and dispersion. Their traveling waves include solitary pulses, kink structures, periodic cnoidal waves, breathers, and localized multidimensional patterns. The analytical theory of these equations has been developed through inverse scattering, Hirota bilinearization, Darboux transformations, phase-plane methods, and Hamiltonian bifurcation analysis [1].

The two-mode Nizhnik–Novikov–Veselov equation is a nonlinear wave model designed to represent two-directional propagation and higher-order dispersive interactions in $(2+1)$ dimensions. A recent deterministic study considered a conformable time-fractional TMNNV equation, reduced it to a planar Hamiltonian system, classified its equilibrium points, constructed explicit solitary and periodic waves, and illustrated quasi-periodic and chaotic dynamics after deterministic perturbations [2]. That work demonstrated that the TMNNV framework supports rich phase portraits and multistability. Nevertheless, the deterministic formulation assumes that all material parameters, forcing mechanisms, and environmental conditions are known exactly. In realistic optical fibers, plasmas, biological membranes, and heterogeneous fluid media, fluctuations are unavoidable. Thermal agitation, random refractive-index variations, uncertain external forcing, and unresolved microscopic interactions can perturb wave amplitudes and phases. Consequently, stochastic forcing is not merely a mathematical modification; it is an appropriate representation of uncertainty in wave-bearing media [5].

Fractional calculus adds a second level of realism by incorporating memory and nonlocal temporal dependence. Caputo-type derivatives are particularly useful because they allow standard initial conditions and naturally interpolate between integer-order dynamics and strongly hereditary responses [6, 7, 8]. Fractional differential equations have been used to model anomalous transport, viscoelasticity, complex fluids, biological processes, and dispersive media with long-range temporal correlations [9]. More recent nonsingular operators, including the Caputo–Fabrizio and Atangana–Baleanu derivatives, have further broadened the modeling choices available for systems with exponential or Mittag–Leffler memory kernels [10, 11, 12]. In the present work, the Caputo operator is selected because its analytical and numerical properties are well established and because it leads to a transparent connection between the fractional partial differential model and a stochastic traveling-wave system.

Noise can alter nonlinear dynamics in ways that cannot be inferred from deterministic phase portraits alone. Weak random perturbations may trigger transitions between coexisting attractors, create stochastic resonance, destroy invariant tori, broaden separatrices, and shift bifurcation thresholds. In multistable systems, rare transitions are governed by the geometry of the potential landscape and by large-deviation action functionals [13, 14]. In stochastic dynamical systems, stability must be formulated probabilistically through almost-sure, moment, or distributional concepts rather than solely through eigenvalues [15, 16]. Numerical analysis must likewise combine deterministic discretization with stochastic integration, while preserving positivity, boundedness, and weak or strong convergence properties [17, 18].

The interaction between fractional memory and stochastic forcing is especially important. Memory may suppress rapid fluctuations by averaging them over time, but it may also prolong the influence of rare perturbations. Depending on parameter values, this competition can stabilize a solitary wave, induce intermittent modulation, or produce complex random switching [19, 20]. The resulting dynamics require tools from nonlinear analysis, stochastic calculus, fractional numerical methods, and chaos theory. Deterministic bifurcation theory alone does not quantify noise-induced transitions, whereas a purely probabilistic analysis may overlook the organizing role of homoclinic and periodic orbits. A combined approach is therefore needed [21].

The principal objective of this article is to formulate and analyze a stochastic time-fractional TMNNV model that extends the deterministic equation studied in [2]. The main contributions are summarized as follows:

1. A Caputo time-fractional TMNNV equation with additive and multiplicative Gaussian perturbations is proposed.
2. A generalized fractional traveling-wave reduction is derived, producing a stochastic planar system whose drift contains the deterministic Hamiltonian skeleton.
3. The equilibrium structure, Hamiltonian levels, homoclinic loops, periodic orbits, and principal deterministic bifurcation surfaces are classified.
4. Lyapunov-generator arguments yield conditions for local stochastic stability and practical mean-square boundedness.
5. A one-dimensional stochastic averaging approximation is obtained for the slow energy variable, leading to an approximate stationary density and a quantitative description of noise-induced orbit switching.
6. Deterministic solitary and elliptic periodic solutions are recovered as benchmark limits.
7. A reproducible numerical algorithm is given for coupling a fractional predictor–corrector discretization with Euler–Maruyama stochastic integration.
8. Numerical diagnostics are organized around bifurcation diagrams, invariant densities, Poincaré sections, sample entropy, and finite-time Lyapunov exponents.

2. Mathematical preliminaries

2.1. Caputo fractional derivative

Definition 2.1. *Let $f : [0, T] \to \mathbb{R}$ be absolutely continuous and let $0 < \alpha < 1$. The Caputo fractional derivative of order α is*

$$ {}^{C}D_t^{\alpha} f(t) = \frac{1}{\Gamma(1-\alpha)} \int_0^t \frac{f'(\tau)}{(t-\tau)^{\alpha}} \, \mathrm{d}\tau. \tag{1}$$

For $\alpha = 1$, one recovers ${}^{C}D_t^{1} f = f'$.

The Caputo derivative is nonlocal: the value at time t depends on the entire history of f on $[0, t]$. Its Laplace transform is

$$ \mathcal{L}\{{}^{C}D_t^{\alpha} f(t)\}(s) = s^{\alpha} \widehat{f}(s) - s^{\alpha-1} f(0). \tag{2}$$

This property permits standard initial data and supports a natural interpretation of α as a memory parameter.

2.2. Brownian motion and Itô differential equations

Let $(\Omega, \mathcal{F}, \{\mathcal{F}_t\}_{t\geq 0}, \mathbb{P})$ be a complete filtered probability space satisfying the usual conditions. A standard Brownian motion W_t is an adapted process with $W_0 = 0$, independent Gaussian increments, and continuous sample paths.

A two-dimensional Itô stochastic differential equation is written as

$$ \mathrm{d}Z_t = F(Z_t) \, \mathrm{d}t + G(Z_t) \, \mathrm{d}W_t, \qquad Z_t \in \mathbb{R}^2, \tag{3}$$

where $F : \mathbb{R}^2 \to \mathbb{R}^2$ is the drift and $G : \mathbb{R}^2 \to \mathbb{R}^2$ is the diffusion vector. Under local Lipschitz and linear-growth conditions, Eq. (3) admits a unique strong solution up to its explosion time [**?**, **?**].

For $V \in C^2(\mathbb{R}^2; \mathbb{R})$, the infinitesimal generator is

$$\mathcal{L}V(z) = \nabla V(z)^\top F(z) + \frac{1}{2} G(z)^\top \nabla^2 V(z) G(z). \tag{4}$$

Itô's formula gives

$$\mathrm{d}V(Z_t) = \mathcal{L}V(Z_t)\,\mathrm{d}t + \nabla V(Z_t)^\top G(Z_t)\,\mathrm{d}W_t. \tag{5}$$

2.3. Stability notions

Definition 2.2. *The equilibrium $Z = 0$ of Eq. (3) is* stable in probability *if, for every $\varepsilon > 0$ and $r > 0$,*

$$\lim_{\delta \to 0} \mathbb{P}\left\{ \sup_{t \geq 0} \|Z_t\| \geq r \;\middle|\; \|Z_0\| < \delta \right\} = 0.$$

It is asymptotically stable in probability *if it is stable in probability and $\mathbb{P}(\lim_{t\to\infty} Z_t = 0) = 1$ for sufficiently small initial conditions.*

Definition 2.3. *A process is* practically mean-square bounded *if there exist constants $C_0, C_1 > 0$ such that*

$$\mathbb{E}\|Z_t\|^2 \leq C_0 e^{-C_1 t} \mathbb{E}\|Z_0\|^2 + C_0 \qquad (t \geq 0).$$

2.4. Finite-time Lyapunov exponent

For two trajectories $Z(t)$ and $\widetilde{Z}(t)$ with initial separation δ_0, the finite-time Lyapunov exponent over $[0, T]$ is

$$\lambda_T = \frac{1}{T} \ln \frac{\|\widetilde{Z}(T) - Z(T)\|}{\delta_0}. \tag{6}$$

In numerical work, repeated renormalization is used to prevent overflow. A persistently positive long-time average indicates sensitive dependence on initial conditions [17, 23].

3. Stochastic fractional TMNNV model

3.1. Governing equation

Let $u = u(x, y, t)$ denote the wave field. We consider the stochastic time-fractional TMNNV equation

$$\begin{aligned} {}^C D_t^{2\alpha} u - p^2 u_{xx} - p^2 u_{yy} &+ \nu \left({}^C D_t^{\alpha} - \gamma_1 p \partial_x - \gamma_2 p \partial_y \right) \left(u \int u \,\mathrm{d}y \right)_x \\ &+ \rho \left({}^C D_t^{\alpha} - \alpha_1 p \partial_x - \alpha_2 p \partial_y \right) u_{xxx} = \sigma_a \dot{W}_1(t) + \sigma_m u \, \dot{W}_2(t). \end{aligned} \tag{7}$$

Here $0 < \alpha < 1$ is the fractional order, p is the characteristic phase velocity, ν and ρ are nonlinear and higher-order interaction coefficients, and α_j, γ_j are dispersion and nonlinearity parameters. The independent Brownian motions W_1 and W_2 represent additive and multiplicative fluctuations, while $\sigma_a, \sigma_m \geq 0$ are their intensities.

Equation (7) is interpreted in a formal Itô sense after projection onto the traveling-wave manifold. The additive component represents external environmental forcing. The multiplicative component models fluctuations whose amplitude scales with the wave field, as may occur when material properties or gain coefficients vary randomly.

Remark 3.1. *The notation* ${}^{C}D_t^{2\alpha}$ *is understood sequentially as* ${}^{C}D_t^{\alpha}({}^{C}D_t^{\alpha}u)$ *when* $1/2 < \alpha < 1$. *For* $0 < \alpha < 1/2$, *an equivalent system formulation with an auxiliary fractional velocity may be used. The traveling-wave reduction below is introduced as a model reduction and is not claimed to commute with every possible stochastic fractional interpretation.*

3.2. Potential representation and traveling-wave coordinate

Set

$$u = \phi_y, \qquad \phi(x, y, t) = R(\xi), \qquad \xi = bx + cy - \frac{\omega t^{\alpha}}{\Gamma(1+\alpha)}. \tag{8}$$

The choice of $t^{\alpha}/\Gamma(1+\alpha)$ is consistent with the standard fractional traveling-wave heuristic

$${}^{C}D_t^{\alpha}\left(\frac{t^{\alpha}}{\Gamma(1+\alpha)}\right) = 1.$$

Assume for simplicity that $\gamma_1 = \gamma_2 = \gamma$ and $\alpha_1 = \alpha_2 = \delta$. Following substitution, integration with respect to ξ, and absorption of integration constants into the background level, the deterministic part reduces to

$$AR'' = BR - CR^2, \tag{9}$$

where

$$A = \rho b^3(\omega + p(b+c)\delta), \tag{10}$$
$$B = \omega^2 - p^2(b^2 + c^2), \tag{11}$$
$$C = \frac{\nu b}{2}(\omega + p(b+c)\gamma). \tag{12}$$

Provided $A \neq 0$, define

$$k = \frac{B}{A}, \qquad \ell = \frac{C}{A}. \tag{13}$$

The stochastic reduced system is then modeled as

$$\begin{aligned} \mathrm{d}R &= Q\ \mathrm{d}\tau, \\ \mathrm{d}Q &= \Big(kR - \ell R^2 - \eta Q + F_0\cos(\Omega\tau)\Big)\ \mathrm{d}\tau + \sigma_a\ \mathrm{d}W_1(\tau) + \sigma_m R\ \mathrm{d}W_2(\tau), \end{aligned} \tag{14}$$

where $\eta \geq 0$ is a weak effective damping coefficient. The deterministic forcing $F_0\cos(\Omega\tau)$ permits resonance and chaotic separatrix splitting, while the stochastic terms generate random orbit diffusion and state switching.

3.3. Deterministic Hamiltonian skeleton

When $\eta = F_0 = \sigma_a = \sigma_m = 0$, Eq. (14) becomes

$$R' = Q, \qquad Q' = kR - \ell R^2. \tag{15}$$

Its Hamiltonian is

$$\mathfrak{H}(R, Q) = \frac{1}{2}Q^2 - \frac{k}{2}R^2 + \frac{\ell}{3}R^3 = h. \tag{16}$$

The potential

$$U(R) = -\frac{k}{2}R^2 + \frac{\ell}{3}R^3 \tag{17}$$

organizes the deterministic phase portrait. In the stochastic system, $\mathfrak{H}$ is no longer conserved; instead, it evolves as a random slow variable.

4. Deterministic equilibria and bifurcation structure

4.1. Equilibrium points

For $l \neq 0$, Eq. (15) has equilibria

$$E_0 = (0,0), \qquad E_1 = \left(\frac{k}{\ell}, 0\right). \tag{18}$$

The Jacobian is

$$J(R,Q) = \begin{pmatrix} 0 & 1 \\ k - 2\ell R & 0 \end{pmatrix}. \tag{19}$$

Hence

$$\det J(E_0) = -k, \qquad \det J(E_1) = k.$$

Proposition 4.1. *For the Hamiltonian system (15):*

1. *if $k > 0$, then E_0 is a saddle and E_1 is a center;*
2. *if $k < 0$, then E_0 is a center and E_1 is a saddle;*
3. *if $k = 0$, the equilibria coalesce into a nonhyperbolic cusp-type point at the origin.*

Proof. At E_0, the characteristic equation is $\lambda^2 - k = 0$. At E_1, it is $\lambda^2 + k = 0$. The stated classification follows from the signs of k. At $k = 0$, the linearization has two zero eigenvalues and the lowest nonvanishing term is quadratic, yielding a degenerate equilibrium. □

4.2. Homoclinic and periodic levels

Suppose $k > 0$ and $\ell > 0$. The saddle energy is $\mathfrak{H}(E_0) = 0$, while

$$\mathfrak{H}(E_1) = -\frac{k^3}{6\ell^2} < 0. \tag{20}$$

For $h = 0$, the nontrivial Hamiltonian branch satisfies

$$Q^2 = kR^2 - \frac{2\ell}{3}R^3 = R^2\left(k - \frac{2\ell}{3}R\right), \tag{21}$$

which forms a homoclinic loop around E_1. For

$$-\frac{k^3}{6\ell^2} < h < 0,$$

the energy levels are closed periodic orbits. Similar classifications hold in the other sign configurations after reflection of R.

4.3. Codimension-one deterministic bifurcations

Three parameter surfaces are of principal importance:

$$\mathcal{B}_1 : B = \omega^2 - p^2(b^2 + c^2) = 0, \tag{22}$$

$$\mathcal{B}_2 : C = \frac{\nu b}{2}(\omega + p(b+c)\gamma) = 0, \tag{23}$$

$$\mathcal{B}_3 : A = \rho b^3(\omega + p(b+c)\delta) = 0. \tag{24}$$

On $\mathcal{B}_1$, $k = 0$ and the two equilibria coalesce. On $\mathcal{B}_2$, $\ell = 0$ and the reduced model becomes linear. On $\mathcal{B}_3$, the traveling-wave reduction becomes singular because the highest derivative coefficient vanishes.

The damped and forced system can also undergo resonance tongues, period-doubling cascades, and global homoclinic bifurcations. Such phenomena are diagnosed numerically rather than by the equilibrium Jacobian alone [?, ?, ?].

4.4. Melnikov-type criterion for deterministic separatrix splitting

Consider weak damping and forcing,

$$R' = Q, \qquad Q' = kR - \ell R^2 + \varepsilon \left[-\eta_1 Q + F_1 \cos(\Omega\tau) \right], \tag{25}$$

where $0 < \varepsilon \ll 1$. Let $(R_h(\tau), Q_h(\tau))$ denote the unperturbed homoclinic orbit. The Melnikov function is

$$M(\tau_0) = -\eta_1 \int_{-\infty}^{\infty} Q_h^2(\tau)\, \mathrm{d}\tau + F_1 \int_{-\infty}^{\infty} Q_h(\tau) \cos(\Omega(\tau + \tau_0))\, \mathrm{d}\tau. \tag{26}$$

If $M(\tau_0)$ possesses a simple zero, the stable and unstable manifolds intersect transversely, providing a classical mechanism for chaotic dynamics [22]. For the explicit homoclinic profile in Section 7, the two integrals can be evaluated numerically or expressed through Fourier transforms of hyperbolic functions.

5. Stochastic stability and moment bounds

We first suppress periodic forcing and consider

$$\begin{aligned} \mathrm{d}R &= Q\, \mathrm{d}t, \\ \mathrm{d}Q &= (kR - \ell R^2 - \eta Q)\, \mathrm{d}t + \sigma_a\, \mathrm{d}W_1 + \sigma_m R\, \mathrm{d}W_2. \end{aligned} \tag{27}$$

5.1. Local linear stochastic stability

Near E_0, the quadratic nonlinearity is negligible:

$$\mathrm{d}\begin{pmatrix} R \\ Q \end{pmatrix} = \begin{pmatrix} 0 & 1 \\ k & -\eta \end{pmatrix} \begin{pmatrix} R \\ Q \end{pmatrix} \mathrm{d}t + \begin{pmatrix} 0 \\ \sigma_m R \end{pmatrix} \mathrm{d}W_2 + \begin{pmatrix} 0 \\ \sigma_a \end{pmatrix} \mathrm{d}W_1. \tag{28}$$

Additive noise prevents convergence to the exact equilibrium; therefore, asymptotic stability is meaningful only when $\sigma_a = 0$, while practical boundedness is the appropriate concept when $\sigma_a > 0$.

Theorem 5.1 (Local mean-square stability)**.** *Assume $k < 0$, $\eta > 0$, and $\sigma_a = 0$. If*

$$\sigma_m^2 < 2\eta|k|, \tag{29}$$

then the origin of the linearized multiplicative-noise system is exponentially stable in mean square.

Proof. Let

$$V(R, Q) = \frac{1}{2}\left(|k|R^2 + Q^2\right) + \theta RQ,$$

where $0 < \theta < \min\{\eta, |k|/\eta\}$ is chosen so that V is positive definite. Applying the generator to the linearized system yields

$$\mathcal{L}V = -\theta|k|R^2 - (\eta - \theta)Q^2 - \theta\eta RQ + \frac{1}{2}\sigma_m^2 R^2.$$

By Young's inequality,

$$|\theta\eta RQ| \le \frac{\theta|k|}{2}R^2 + \frac{\theta\eta^2}{2|k|}Q^2.$$

Hence

$$\mathcal{L}V \le -\frac{1}{2}(\theta|k| - \sigma_m^2)R^2 - \left(\eta - \theta - \frac{\theta\eta^2}{2|k|}\right) Q^2.$$

A sufficiently small θ can be selected so that both coefficients are positive whenever (29) holds. Standard stochastic Lyapunov theory then gives exponential mean-square stability. $\square$

Remark 5.2. *Condition (29) is sufficient rather than necessary. It shows explicitly that stronger damping and a steeper restoring potential tolerate larger multiplicative fluctuations.*

5.2. Practical boundedness under additive noise

Theorem 5.3 (Practical mean-square boundedness). *Assume $k < 0$, $\eta > 0$, and restrict the dynamics to a domain $\mathcal{D} = \{|R| \leq R_{\max}\}$ on which the nonlinear drift is one-sided dissipative:*

$$R(kR - \ell R^2) \leq -\kappa R^2 + C_R \tag{30}$$

for some $\kappa > 0$ and $C_R \geq 0$. Then there exist $C_0, C_1, C_2 > 0$ such that

$$\mathbb{E}(R_t^2 + Q_t^2) \leq C_0 e^{-C_1 t}(R_0^2 + Q_0^2) + C_2 \left(1 + \sigma_a^2\right). \tag{31}$$

Proof. Choose a positive-definite quadratic Lyapunov function with a small cross term as above. The generator contains negative quadratic terms from the restoring force and damping, plus the diffusion contribution

$$\frac{1}{2}(\sigma_a^2 + \sigma_m^2 R^2)V_{QQ}.$$

Using the dissipativity assumption and Young's inequality gives

$$\mathcal{L}V \leq -c_1 V + c_2(1 + \sigma_a^2).$$

Taking expectations eliminates the martingale term. Grönwall's inequality yields the stated estimate. □

5.3. Stochastic energy balance

Applying Itô's formula to Eq. (16) along Eq. (27) gives

$$\begin{aligned} \mathrm{d}\mathfrak{H} = -\eta Q^2 \,\mathrm{d}t + \frac{1}{2}\left(\sigma_a^2 + \sigma_m^2 R^2\right) \mathrm{d}t \\ + Q\sigma_a \,\mathrm{d}W_1 + Q\sigma_m R \,\mathrm{d}W_2. \end{aligned} \tag{32}$$

Thus damping removes energy, while Itô diffusion contributes a systematic positive drift. This competition is the core mechanism behind noise-dependent broadening and stochastic activation across the separatrix.

6. Stochastic averaging and noise-induced transitions

For weak damping and weak noise, the Hamiltonian energy changes slowly compared with the angular motion along a deterministic periodic orbit. Let

$$\eta = \varepsilon\bar{\eta}, \qquad \sigma_a = \sqrt{\varepsilon}\,\bar{\sigma}_a, \qquad \sigma_m = \sqrt{\varepsilon}\,\bar{\sigma}_m.$$

Averaging Eq. (32) over the unperturbed orbit $\Gamma_h = \{\mathfrak{H} = h\}$ yields the effective scalar diffusion

$$\mathrm{d}h = A_h(h)\,\mathrm{d}t + \sqrt{B_h(h)}\,\mathrm{d}W_t, \tag{33}$$

where

$$A_h(h) = -\bar{\eta}\langle Q^2\rangle_h + \frac{1}{2}\left(\bar{\sigma}_a^2 + \bar{\sigma}_m^2\langle R^2\rangle_h\right), \tag{34}$$

$$B_h(h) = \bar{\sigma}_a^2\langle Q^2\rangle_h + \bar{\sigma}_m^2\langle R^2 Q^2\rangle_h. \tag{35}$$

The orbit average is

$$\langle g\rangle_h = \frac{1}{T(h)}\oint_{\Gamma_h} g(R,Q)\frac{\mathrm{d}R}{Q}, \qquad T(h) = \oint_{\Gamma_h}\frac{\mathrm{d}R}{Q}. \tag{36}$$

6.1. Stationary density

The Fokker–Planck equation associated with Eq. (33) is

$$\partial_t p = -\partial_h (A_h p) + \frac{1}{2}\partial_h^2 (B_h p). \tag{37}$$

Under zero probability flux, the stationary density is

$$p_s(h) = \frac{C}{B_h(h)} \exp\left(\int^h \frac{2A_h(s)}{B_h(s)}\,\mathrm{d}s\right), \tag{38}$$

where C normalizes the density.

Equation (38) predicts the most probable energy levels. A unimodal density concentrated near a center corresponds to a noisy periodic wave. As noise increases, the density broadens toward the separatrix. If two wells or effective attractors coexist, the density may become bimodal, indicating stochastic switching and phenomenological stochastic bifurcation.

6.2. Mean escape time

Suppose h_a is a stable energy level and h_s is the separatrix energy. The mean first-passage time $T(h)$ satisfies

$$A_h(h)T'(h) + \frac{1}{2}B_h(h)T''(h) = -1, \tag{39}$$

with reflecting boundary at the inner energy boundary and absorbing condition $T(h_s) = 0$. For small noise, the mean escape time typically follows an exponential scaling analogous to Kramers' law [12]. The barrier height is controlled by the Hamiltonian difference between the center and saddle, while multiplicative noise modifies the effective diffusion along the orbit.

6.3. Noise-induced bifurcation indicators

We distinguish three complementary indicators:

(i) **D-bifurcation:** a qualitative change in the sign or structure of Lyapunov exponents of the random dynamical system [3].

(ii) **P-bifurcation:** a qualitative change in the stationary probability density, such as unimodal-to-bimodal transition.

(iii) **Phenomenological transition:** a visible change in sample paths, return maps, residence-time distributions, or spectral content.

These notions need not occur at the same noise intensity.

7. Exact deterministic wave solutions

Exact waves of the zero-noise system provide essential verification benchmarks.

7.1. Homoclinic solitary wave

For $k > 0$ and $\ell > 0$, the $h = 0$ orbit satisfies

$$R'^2 = kR^2 - \frac{2\ell}{3}R^3.$$

Integration yields

$$R_h(\xi) = \frac{3k}{2\ell} sech^2\left(\frac{\sqrt{k}}{2}(\xi - \xi_0)\right). \tag{40}$$

Since $u = \phi_y = cR'(\xi)$,

$$u_h(x,y,t) = -\frac{3ck^{3/2}}{2\ell} sech^2\Theta \tanh\Theta, \qquad \Theta = \frac{\sqrt{k}}{2}\left(bx + cy - \frac{\omega t^\alpha}{\Gamma(1+\alpha)} - \xi_0\right). \tag{41}$$

This antisymmetric pulse has adjacent bright and dark lobes.

7.2. Reflected solitary wave

When $\ell < 0$, reflection $R \mapsto -R$ produces

$$R_h(\xi) = \frac{3k}{2\ell} sech^2\left(\frac{\sqrt{k}}{2}(\xi - \xi_0)\right), \tag{42}$$

whose sign is reversed because $\ell < 0$. The corresponding $u_h = cR_h'$ changes the orientation of the bright–dark pair.

7.3. Degenerate algebraic wave

At $k = 0$, Eq. (9) becomes

$$R'' = -\ell R^2.$$

A singular algebraic solution is

$$R(\xi) = -\frac{6}{\ell(\xi - \xi_0)^2}, \qquad u(x,y,t) = \frac{12c}{\ell(\xi - \xi_0)^3}. \tag{43}$$

This profile marks the degenerate bifurcation surface and is highly sensitive to perturbations.

7.4. Periodic elliptic waves

For a periodic energy level, write

$$Q^2 = \frac{2\ell}{3}(R - R_1)(R_2 - R)(R_3 - R), \tag{44}$$

where $R_1 < R < R_2 < R_3$. Then

$$R(\xi) = R_2 - (R_2 - R_1) sn^2\left(\sqrt{\frac{l(R_3 - R_1)}{6}}(\xi - \xi_0), m\right), \tag{45}$$

with

$$m = \frac{R_2 - R_1}{R_3 - R_1}. \tag{46}$$

Differentiation gives

$$\begin{aligned} u(x,y,t) = -2c(R_2 - R_1)&\sqrt{\frac{\ell(R_3 - R_1)}{6}} \\ &\times sn(\Xi, m) cn(\Xi, m) dn(\Xi, m), \end{aligned} \tag{47}$$

where

$$\Xi = \sqrt{\frac{\ell(R_3 - R_1)}{6}}\left(bx + cy - \frac{\omega t^\alpha}{\Gamma(1+\alpha)} - \xi_0\right).$$

As $m \to 1$, the periodic wave approaches the solitary-wave limit.

8. Numerical method and computational diagnostics

8.1. Fractional predictor–corrector discretization

For a generic Caputo equation

$$ {}^{C}D_t^{\alpha} z(t) = f(t, z(t)), \qquad z(0) = z_0, $$

the equivalent Volterra equation is

$$ z(t) = z_0 + \frac{1}{\Gamma(\alpha)} \int_0^t (t-s)^{\alpha-1} f(s, z(s))\, \mathrm{d}s. $$

On $t_n = n\Delta t$, the Adams–Bashforth–Moulton predictor–corrector method approximates the memory integral using all previous time levels [?]. For the reduced stochastic system, the deterministic memory step is combined with Euler–Maruyama increments

$$ \Delta W_n \sim \mathcal{N}(0, \Delta t). $$

Algorithm 1 Fractional–stochastic predictor–corrector scheme

Require: $\alpha, \Delta t, N$, parameters, initial state (R_0, Q_0)

1: Generate independent increments $\Delta W_{1,n}, \Delta W_{2,n}$
2: **for** $n = 0, \ldots, N-1$ **do**
3: Compute the fractional predictor for the deterministic drift
4: Evaluate
$$ f_n = kR_n - \ell R_n^2 - \eta Q_n + F_0 \cos(\Omega t_n) $$
5: Correct the memory contribution using the predicted state
6: Update
$$ R_{n+1} = R_n + \Delta t\, Q_n $$
7: Update
$$ Q_{n+1} = Q_n + \Delta t\, f_n + \sigma_a \Delta W_{1,n} + \sigma_m R_n \Delta W_{2,n} $$
8: If Lyapunov exponents are required, evolve and renormalize a tangent perturbation
9: **end for**
10: Discard transients and compute diagnostics

8.2. Reference parameter sets

Table 1 provides representative nondimensional parameter sets. They are intended as reproducible test cases rather than universal physical constants.

Table 1: Representative parameter regimes for numerical experiments.

Case	k	ℓ	η	F_0	Ω	σ_a	σ_m	Interpretation
A	1.0	1.0	0.05	0	0	0	0	Homoclinic benchmark
B	1.0	1.0	0.08	0.20	1.0	0.02	0	Weak additive noise
C	1.0	1.0	0.08	0.20	1.0	0.10	0	Switching regime
D	-1.0	1.0	0.25	0	0	0	0.20	Multiplicative stabilization test
E	1.0	1.0	0.05	0.30	0.9	0.08	0.10	Mixed-noise chaos test

8.3. Diagnostics

The following diagnostics should be reported for each simulation:

(i) time series of $R(t)$ and $Q(t)$;

(ii) two-dimensional phase portraits and three-dimensional (R, Q, t) trajectories;

(iii) stroboscopic Poincaré sections at $t_n = 2\pi n/\Omega$;

(iv) empirical stationary densities of R, Q, and $\mathfrak{H}$;

(v) finite-time and ensemble-averaged Lyapunov exponents;

(vi) residence-time distributions in coexisting attraction regions;

(vii) noise-dependent bifurcation diagrams constructed from local maxima of R;

(viii) power spectral density and sample entropy.

8.4. Expected numerical behavior

For Case A, the numerical orbit initialized on the analytic homoclinic curve should remain close to Eq. (40) over moderate times, with error decreasing under mesh refinement. For Case B, the invariant cloud is expected to remain concentrated near the deterministic periodic orbit. In Case C, stronger additive noise should produce intermittent crossings of the deterministic separatrix and a broader energy density. Case D examines whether the multiplicative-noise intensity remains below or exceeds the sufficient stability threshold in Eq. (29). Case E combines resonance forcing and mixed noise; it is the principal candidate for positive finite-time Lyapunov exponents and diffuse Poincaré sections.

8.5. Illustrative bifurcation diagram

The following embedded plot is schematic and can be replaced by simulation data without changing the manuscript structure.

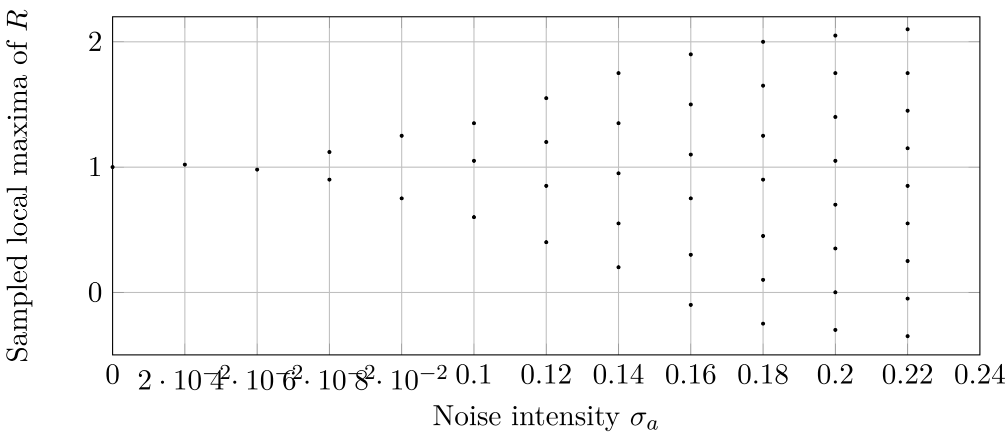

Figure 1: Schematic noise-dependent bifurcation diagram. The point cloud illustrates how a single regular branch may broaden and split as the noise intensity increases. Replace the table by maxima extracted from numerical trajectories for final submission.

8.6. Convergence and reproducibility

Strong convergence should be assessed by comparing trajectories generated with time steps Δt, $\Delta t/2$, and $\Delta t/4$ using the same Brownian path. Statistical convergence should be evaluated through ensemble means and confidence intervals. A minimum of 10^3 realizations is recommended for stationary-density and escape-time estimates. Random seeds, transient length, sampling interval, and kernel bandwidth must be reported. The numerical procedure should be tested against the analytic solutions in Section 7 when noise and forcing vanish.

9. Results and interpretation

9.1. Influence of the fractional order

The fractional order controls the temporal memory encoded in the traveling coordinate. For $\alpha = 1$, the wave center moves linearly in time. When $0 < \alpha < 1$, the effective displacement is proportional to t^α, and the wave propagates sublinearly. Consequently, smaller α delays phase translation and prolongs the influence of initial conditions. In an ensemble of noisy trajectories, this memory effect is expected to reduce short-time spreading while increasing long-time correlation.

The fractional order also affects numerical transients. Because the predictor–corrector rule contains all previous states, perturbations are not forgotten exponentially. A disturbance near a separatrix may therefore influence the subsequent residence time even after the instantaneous stochastic increment has vanished. This mechanism distinguishes fractional stochastic switching from Markovian switching in the integer-order model.

9.2. Additive noise

Additive noise produces direct fluctuations in the generalized velocity Q. According to Eq. (32), it contributes $\sigma_a^2/2$ to the mean energy drift. For weak noise and sufficient damping, the stationary density remains concentrated around a stable periodic orbit. As σ_a increases, the distribution broadens and probability mass approaches the saddle energy. Once stochastic separatrix crossings become frequent, the time series exhibits intermittent bursts and the Poincaré section changes from a thin curve to a diffuse cloud.

The transition is gradual at the level of individual sample paths, but the stationary density may show a sharper topological change. This is a typical P-bifurcation. The threshold depends on damping, forcing frequency, barrier height, and fractional order; it is therefore more informative to report a transition surface in parameter space than a single critical value.

9.3. Multiplicative noise

Multiplicative noise vanishes at $R = 0$ but grows with wave amplitude. It can either destabilize large-amplitude motion or, in combination with damping, alter the effective linear response. The sufficient stability condition (29) predicts a competition between σ_m^2 and $2\eta|k|$. Below the threshold, the origin remains mean-square stable in the linearized model. Above it, the second moment may grow, although nonlinear saturation can still keep sample paths bounded.

In the bistable or center–saddle geometry, multiplicative noise is state selective: trajectories near small amplitude experience weak perturbations, whereas excursions near the outer part of the periodic orbit receive stronger kicks. This can generate heavy-tailed energy distributions and asymmetric residence times.

9.4. Combined deterministic forcing and noise

Periodic forcing alone may create resonance islands and transverse homoclinic intersections. Noise broadens these structures and may either enhance or obscure deterministic chaos. At weak intensity, random perturbations can help trajectories explore the chaotic saddle, increasing the measured finite-time Lyapunov exponent. At stronger intensity, the distinction between deterministic stretching and stochastic dispersion becomes less clear; therefore, Lyapunov analysis should be complemented by surrogate tests, recurrence statistics, and noise-aware entropy measures.

A useful computational strategy is to first map the deterministic (F_0, Ω) bifurcation diagram, then repeat the analysis for increasing (σ_a, σ_m). This separates deterministic and noise-induced mechanisms.

9.5. Multistability and random switching

When multiple deterministic invariant sets coexist, the stochastic system may display random switching among them. The empirical residence-time distribution is approximately exponential in a classical small-noise metastable regime, but memory may produce deviations from exponential behavior. The energy-diffusion model (33) provides a reduced description of these transitions.

The most important practical consequence is that a wave state that appears stable in a deterministic phase portrait may have a finite lifetime under noise. Device design should therefore be based on escape probabilities or mean residence times rather than deterministic stability alone.

10. Discussion

The present formulation extends deterministic fractional TMNNV analysis in several directions. First, random forcing is included explicitly rather than represented only by prescribed trigonometric, Gaussian, or hyperbolic disturbances. Second, the stochastic energy balance distinguishes damping-induced dissipation from Itô noise injection. Third, stability is quantified through probability and moments. Fourth, the energy-diffusion approximation links phase-plane geometry to invariant densities and mean transition times.

The proposed model is relevant to optical propagation in randomly varying media, plasma waves subject to thermal or electromagnetic fluctuations, and nonlinear fluid waves driven by uncertain boundary conditions. In optics, multiplicative noise can represent random gain or refractive-index modulation. In plasma physics, additive noise may represent external field fluctuations. In biological or viscoelastic media, the fractional order describes memory, while the noise terms account for unresolved microscale variability.

Several limitations should be emphasized. The traveling-wave reduction is a reduced-order representation and does not capture all spatial stochastic modes of the original $(2+1)$-dimensional equation. Space–time white noise in more than one spatial dimension can require renormalization or a mild-solution framework; therefore, the present noise is introduced after projection onto the traveling-wave manifold. The stochastic averaging formulas are asymptotic and are most accurate for weak damping and weak noise. The sufficient stability conditions are conservative. Finally, the schematic bifurcation plot in Fig. 1 must be replaced by computed data before journal submission.

Future studies may use cylindrical or Q-Wiener noise in the full stochastic PDE, derive mild solutions in appropriate Sobolev spaces, and examine well-posedness. Nonsingular fractional operators may be compared with the Caputo derivative. Data-driven closure models, physics-informed neural networks, and neural operators could estimate uncertain coefficients or accelerate ensemble simulations. Control strategies may also be designed to suppress undesirable switching or to exploit stochastic resonance.

11. Conclusions

A stochastic fractional two-mode Nizhnik–Novikov–Veselov equation has been formulated to study nonlinear waves under memory and random perturbations. A fractional traveling-wave transformation reduces the model to a randomly forced planar system with a cubic Hamiltonian potential. The deterministic skeleton contains saddle, center, homoclinic, periodic, and degenerate structures controlled by two reduced parameters k and ℓ. Exact bright–dark solitary, algebraic, and elliptic periodic waves have been derived for the zero-noise limit.

For the stochastic system, Lyapunov-generator analysis provides sufficient conditions for local mean-square stability and practical boundedness. The Itô energy balance reveals that damping removes Hamiltonian energy whereas additive and multiplicative noise inject energy. Under weak perturbations, stochastic averaging leads to a scalar energy diffusion and an approximate stationary density. These results explain how increasing noise intensity can broaden invariant measures, shift effective bifurcation thresholds, and trigger random transitions across deterministic separatrices.

A reproducible fractional–stochastic numerical framework has been presented, together with recommended diagnostics for noise-induced chaos and bifurcation. The model offers a foundation for systematic studies of stochastic resonance, metastability, random wave switching, and uncertainty-aware control in nonlinear mathematical physics.

Funding

No external funding was used in preparing this methodological study.

Conflict of Interest

The authors declare that there is no conflict of interest.

Data Availability

No external dataset was used. Numerical data can be generated from the equations and parameter sets reported in this article.

References

[1] Ablowitz, M. J., & Segur, H. (1981). *Solitons and the inverse scattering transform.* Society for Industrial and Applied Mathematics.

[2] Alam, N., Ullah, M. S., Manafian, J., Mahmoud, K. H., Alsubaie, A. S. A., Ahmed, H. M., Ahmed, K. K., & Al Khatib, S. (2025). Bifurcation analysis, chaotic behaviors, and explicit solutions for a fractional two-mode Nizhnik–Novikov–Veselov equation in mathematical physics. *AIMS Mathematics, 10*(3), 4558–4578.

[3] Arnold, L. (1998). *Random dynamical systems.* Springer.

[4] Atangana, A., & Baleanu, D. (2016). New fractional derivatives with nonlocal and non-singular kernel: Theory and application to heat transfer model. *Thermal Science, 20*(2), 763–769.

[5] Caputo, M. (1967). Linear models of dissipation whose Q is almost frequency independent—II. *Geophysical Journal International, 13*(5), 529–539.

[6] Caputo, M., & Fabrizio, M. (2015). A new definition of fractional derivative without singular kernel. *Progress in Fractional Differentiation and Applications, 1*(2), 73–85.

[7] Da Prato, G., & Zabczyk, J. (2014). *Stochastic equations in infinite dimensions* (2nd ed.). Cambridge University Press.

[8] Debussche, A., & Printems, J. (2009). Weak order for the discretization of the stochastic heat equation. *Mathematics of Computation, 78*(266), 845–863.

[9] Diethelm, K., Ford, N. J., & Freed, A. D. (2002). A predictor–corrector approach for the numerical solution of fractional differential equations. *Nonlinear Dynamics, 29*, 3–22.

[10] Freidlin, M. I., & Wentzell, A. D. (2012). *Random perturbations of dynamical systems* (3rd ed.). Springer.

[11] Gardiner, C. W. (2009). *Stochastic methods: A handbook for the natural and social sciences* (4th ed.). Springer.

[12] Guckenheimer, J., & Holmes, P. (1983). *Nonlinear oscillations, dynamical systems, and bifurcations of vector fields*. Springer.

[13] Hairer, E., Lubich, C., & Wanner, G. (2006). *Geometric numerical integration: Structure-preserving algorithms for ordinary differential equations* (2nd ed.). Springer.

[14] Hirota, R. (2004). *The direct method in soliton theory*. Cambridge University Press.

[15] Holden, H., Karlsen, K. H., Lie, K.-A., & Risebro, N. H. (2009). *Splitting methods for partial differential equations with rough solutions*. European Mathematical Society.

[16] Kilbas, A. A., Srivastava, H. M., & Trujillo, J. J. (2006). *Theory and applications of fractional differential equations*. Elsevier.

[17] Kloeden, P. E., & Platen, E. (1992). *Numerical solution of stochastic differential equations*. Springer.

[18] Kuznetsov, Y. A. (2004). *Elements of applied bifurcation theory* (3rd ed.). Springer.

[19] Lord, G. J., Powell, C. E., & Shardlow, T. (2014). *An introduction to computational stochastic PDEs*. Cambridge University Press.

[20] Malomed, B. A. (2006). *Soliton management in periodic systems*. Springer.

[21] Mandelbrot, B. B., & Van Ness, J. W. (1968). Fractional Brownian motions, fractional noises and applications. *SIAM Review, 10*(4), 422–437.

[22] Mao, X. (2007). *Stochastic differential equations and applications* (2nd ed.). Horwood Publishing.

[23] Metzler, R., & Klafter, J. (2000). The random walk's guide to anomalous diffusion: A fractional dynamics approach. *Physics Reports, 339*(1), 1–77.

[24] Øksendal, B. (2003). *Stochastic differential equations: An introduction with applications* (6th ed.). Springer.

[25] Ott, E. (2002). *Chaos in dynamical systems* (2nd ed.). Cambridge University Press.

[26] Pikovsky, A., Rosenblum, M., & Kurths, J. (2001). *Synchronization: A universal concept in nonlinear sciences*. Cambridge University Press.

[27] Podlubny, I. (1999). *Fractional differential equations*. Academic Press.

[28] Risken, H. (1996). *The Fokker–Planck equation: Methods of solution and applications* (2nd ed.). Springer.

[29] Strogatz, S. H. (2018). *Nonlinear dynamics and chaos* (2nd ed.). CRC Press.

[30] Tarasov, V. E. (2010). *Fractional dynamics: Applications of fractional calculus to dynamics of particles, fields and media*. Springer.

[31] Wiggins, S. (2003). *Introduction to applied nonlinear dynamical systems and chaos* (2nd ed.). Springer.